Satellite Observed Salinity Distributions at High Latitudes in the Northern Hemisphere: A Comparison of Four Products

Cynthia Garcia-Eidell[1,2]

cynthia.o.garcia@nasa.gov

Josefino C. Comiso[1,5]

josefino.c.comiso@nasa.gov

Emmanuel Dinnat[1,3]

emmanuel.dinnat@nasa.gov

Ludovic Brucker[1,4]

ludovic.brucker@nasa.gov

[1]NASA Goddard Space Flight Center,

Cryospheric Sciences Laboratory, Greenbelt, MD 20771, USA

[2]Wyle Science Technology and Engineering,

2400 NASA Parkway, Houston, TX 77058, USA

[3]Center of Excellence in Earth Systems Modeling and Observation,

Chapman University, Orange, CA 92866, USA

[4]Universities Space Research Association, Goddard Earth Sciences Technology and Research Studies and Investigations, Columbia, MD 21044, USA

[5]Corresponding Author

Submitted to Journal of Geophysical Research –Oceans on 9 June 2017

Revised on 11 August 2017, Accepted on 28 August 2017

Key Points: 1. Satellite-derived sea surface salinity in the Arctic region from four products, three from Aquarius and one from SMOS are compared.

2. Validation studies indicate good agreement of satellite data with in situ salinity measurements and usefulness of the data in monitoring spatial and temporal variability in the Arctic.

3. Significant discrepancies in the spatial and temporal distribution are observed between the products as a result of differences in noise reduction and smoothing and in the masking of land and sea ice.

4. All products showed general consistency in capturing sea surface salinity's seasonality and interannual variability in the Arctic if similar data quality control is applied.

ABSTRACT

Global surface ocean salinity measurements have been available since the launch of SMOS in 2009 and coverage was further enhanced with the launch of Aquarius in 2011. In the polar regions where spatial and temporal changes in sea surface salinity (SSS) are deemed important, the data has not been as robustly validated because of the paucity of in situ measurements. This study presents a comparison of four SSS products in the ice-free Arctic region, three using Aquarius data and one using SMOS data. The accuracy of each product is assessed through comparative analysis with ship and other in situ measurements. Results indicate RMS errors ranging between 0.33 and 0.89 psu. Overall, the four products show generally good consistency in spatial distribution with the Atlantic side being more saline than the Pacific side. A good agreement between the ship and satellite measurements were also observed in the low salinity regions in the Arctic Ocean, where SSS in situ measurements are usually sparse, at the end of summer melt seasons. Some discrepancies including biases of about 1 psu between the products in spatial and temporal distribution are observed. These are due in part to differences in retrieval techniques, geophysical filtering, and sea ice and land masks. The monthly SSS retrievals in the Arctic from 2011 to 2015 showed variations (within ~1 psu) consistent with effects of sea ice seasonal cycles. This study indicates that spaceborne observations capture the seasonality and interannual variability of SSS in the Arctic with reasonably good accuracy.

1. Introduction

Salinity has been regarded as one of the key geophysical parameters that affect ocean circulation, hydrological cycle, ocean ecology and changes in the climate. Together with temperature, it drives the thermohaline circulation of the ocean, which influences the transport of heat, energy and humidity thereby modulating climate [*Aagard et al.*, 1985; *Broecker,* 1997]. Salinity is also an abiotic factor that shapes the ecological landscape of the environment and the distribution of nutrients that are consumed by algae and other biological species in the ocean. It has also been used as a tracer of water mass movement and advection characteristics of surface water [*Durack et al.,* 2012]. Despite the importance of monitoring salinity, knowledge of its global distribution and the variations of such distribution both in space and time has been inadequate. Ocean-mixing processes and freshwater discharge mechanisms remain poorly understood notwithstanding possible connections of warming with high-latitude freshening [*Schmitt*, 2008]. Such global distributions are not expected to be spatially uniform on account of many factors. For example, salinity is low in some areas because of the transport of freshwater through precipitation, river runoff, and in higher latitudes, ice melt from sea ice and land ice [*Lehner et al.,* 2012; *Nummelin et al.,* 2016]. It is also relatively higher in areas where there is excessive evaporation or sea ice production.

The lack of in situ salinity data is an even more serious challenge in the Arctic region due to the very sparse sampling partly due to the harsh environment, adverse weather conditions and the presence of sea ice. Such limitations are unfortunate because large spatial and temporal variabilities in sea surface salinity (SSS) are expected in the Arctic region because of the highly seasonal sea ice cover and a summer ice minimum that has been observed to be changing rapidly [*Vaughan et al.,* 2014*; Cavalieri and Parkinson,* 2012*; Comiso et al.,* 2008]. In addition, glacial melt contribution from the Greenland ice sheet has been increasing significantly from 170 to 360 km^3/year [*Khan et al.,* 2014]. This mass loss is expected to significantly impact the thermohaline circulation and as *Dukhovskoy et al.,* in 2016 estimates, surplus Greenland freshwater flux should cause salinity decrease of 0.06-0.08 in the sub-Arctic seas. Such changes are expected to cause variations in salinity and temperature distributions that could affect the circulation and productivity of the Arctic Ocean and surrounding seas. The observed salinity anomalies in the Arctic has also been linked to changes in the phase of the Arctic Oscillation [*Houssais et al*., 2007].

Fortuitously, satellite L-band sensors (operating at a frequency of ~1.4 GHz) have been developed in recent years and are well suited for monitoring global distributions of SSS at a reasonable temporal resolution of about one week or longer. The earliest of these is the European Space Agency's (ESA) Soil Moisture and Ocean Salinity (SMOS), which is a purely passive system launched on 02 November 2009. The next one was the Aquarius SAC-D, launched on 10 June 2011, which was a joint venture of National Aeronautics and Space Administration's (NASA) and Argentina's Comision Nacional de Actividades Espaciales (CONAE). Unfortunately, Aquarius ceased operation on 07 June 2015 but NASA's SMAP (Soil Moisture Active Passive) was launched on 31 January 2015. The latter is meant to measure soil moisture but also has the capability of providing estimates of surface salinity. The important question is how accurately the salinity distribution can be derived especially in the relatively cold high latitude waters where retrieval techniques have the most problem.

The primary goal of this study is to evaluate and assess the accuracy of spatial and temporal variabilities of the SSS in the Arctic region as derived from satellite data. To achieve this goal, a comparative study is performed using four SSS products from Aquarius and SMOS at high latitudes in the Northern Hemisphere. These products are compared with available ship thermosalinograph (TSG) measurements and with quality-controlled CORA (COriolis Ocean database for ReAnalysis) [*Szekely et al*, 2015; *Cabanes et al*, 2013] in situ dataset to establish confidence about the validity of the techniques used in creating the products from the L-band satellite observations. Through this process we assess the uncertainties associated with these existing products to ensure proper interpretation of the results of analysis. Data from 2011 to 2015 are then analyzed to study the seasonal and yearly changes in the spatial distribution of SSS during this period as consistently revealed by satellite data.

2. Methodology and Satellite Data Products

2.1. Retrieval of SSS from Satellite Data

Satellite passive microwave systems have been around since the 1970s but have not been used until recently for salinity measurements because the systems did not have the low-frequency requirement needed to be sensitive enough to measure SSS. The right wavelength and algorithms are needed to remove ambiguities and be able to establish that the geophysical parameter that is being measured is SSS. The ambiguities are associated with the influence of many other factors such as sea surface temperature (SST), roughness, atmospheric conditions and others on the brightness temperature of the surface. Although salinity can be derived through the sole use of data from passive microwave radiometers, further improvements in accuracy is expected through a combined passive and active system as will be discussed below.

The techniques for the retrieval of salinity from passive microwave data have been discussed in many publications that includes the Algorithm Theoretical Basis Documents (ATBD) [e.g., *Le Vine et al.*, 2011; *Brucker et al*., 2014; *Wentz and Yueh*, 2011; *Wentz and Le Vine*, 2012; *Yueh et al.*, 2014; *Meissner et al.*, 2014]. The physics of the techniques are basically the same and make use of a radiative transfer forward model to retrieve the surface brightness temperature (T_B) from Aquarius (and SMOS) measurements. The contaminations to the measured signal due to radiation from the galaxy, sun, moon and Earth's atmosphere are estimated [*Dinnat and Le Vine*, 2008; *Dinnat et al.*, 2009] and deducted from measured antenna temperatures (T_A). For the Aquarius algorithm, an antenna pattern correction is applied to remove cross-polarization effects and Faraday rotation is removed using the 2nd and 3rd Stokes parameters [*Yueh*, 2000; *Le Vine et al.*, 2013]. To correct for atmospheric contributions, National Centers for Environmental Prediction (NCEP) profiles of temperature, pressure, liquid water and humidity were interpolated to the location of Aquarius measurements. Reynolds OI SST product is used as the ancillary SST field. After the corrections are applied, the resulting term is the brightness temperature of the ocean surface, T_B that is used to obtain the surface salinity.

In the microwave frequency region, the Stefan-Boltzmann's Law reduces to Rayleigh-Jeans approximation, which is given by the equation:

$$T_B = \in * SST \qquad (1)$$

where SST and $\in$ are the temperature and emissivity of the surface, respectively. The emissivity is the key radiative property of the surface and contains the information associated with salinity in ocean-covered regions. The emissivity, which depends on incident angle, can be inferred from the surface reflectivity (R) as:

$$\in = 1 - R \qquad (2)$$

with R a function of the surface roughness, incidence angle and sea water dielectric constant, ε, which depends on SST, SSS and radio frequency.

All algorithms have to account for the impact of surface roughness in order to retrieve SSS, see examples in [*Meissner et al.*, 2014; *Yueh et al., 2014*]. Aquarius makes use of its active measurements from its collocated radar scatterometer to improve the surface roughness correction, which is an asset that neither SMOS nor SMAP have (SMAP's radar failed three months into the mission in July 2015). Remote sensing theory and airborne experiments have demonstrated the importance of the radar in providing complementary information about the wind and surface roughness for L-band remote sensing [*Yueh et al.*, 2001; *Yueh et al.*, 2010; *Martin et al.*, 2014] and uncertainty on Aquarius SSS retrievals is significantly reduced with the inclusion of radar observations (see Table 3 in *Meissner et al.*, 2014).

It is apparent that the retrieval of SSS requires the knowledge of many parameters some of which need to be estimated through models or special techniques. The models and techniques are not as well validated in the Arctic as in other regions because of the paucity of data as illustrated in the map shown in Figure 1a. The map shows data points from Argo buoys (in blue) and other in situ data sources (in red) and indicates that the locations of most of the in-situ data are primarily in the subarctic regions while there is hardly any data north of 60°N. The map also serves as a location map that indicates where the various seas in the region are located as well as the mouth of key rivers where significant amounts of fresh water are introduced to the Arctic Basin.

The dependence of T_B at 1.4 GHz (L-band) and 35° incidence angle on SST for different values of SSS from 25 psu to 29 psu are illustrated in Figure 1b and 1c for vertical and horizontal polarizations, respectively. The relatively low sensitivity of SSS at low temperature waters compared to those in warmer waters are apparent making the ability to obtain accurate salinity a bigger challenge in the Arctic (i.e., cold) region than in lower latitude regions. The two plots also show that at a given temperature, T_B decreases as SSS increases. It can be seen that the SSS spread is wider in the vertical component than in the horizontal component, thus, making the former slightly more sensitive to SSS changes. In addition to this, *Brucker, et al.*, [2014] and *Dinnat and Brucker,* [2017] showed that T_B is also highly sensitive to the presence of sea ice due to the differences in emissivity, which can be interpreted as an erroneous decrease of SSS or freshening.

2.2. Data Source and Data Products

The key sources of satellite data that are currently used for the retrieval of SSS are Aquarius and SMOS sensors. Recent launch of SMAP provides a third source but since advanced processing is still in progress, SSS data are not yet publicly available at the time of this study and therefore only data from Aquarius and SMOS were used.

The Aquarius satellite is composed of three radiometers and one scatterometer operating at L-band. The radiometers operate at 1.414 GHz and their beams have incidence angles of 29.2°, 38.48° and 46.3°, providing us with a total cross track of 370 km and footprints of 74 km x 94 km, 84 km x 120 km, and 96 km x 156 km, respectively. Aquarius' scatterometer operates at 1.26 GHz and is primarily used to account for surface roughness correction in the salinity retrievals. With a swath width of 390 km global coverage by Aquarius is achieved in seven days but since the satellite is polar orbiting with an inclination angle of 98° there is more coverage in the polar regions and our domain is completely covered every 3 days. The mission's required accuracy is 0.2 psu after averaging over a month at a resolution of 150 km x 150 km in global open oceans. This study made use of three Aquarius SSS products, namely: (1) Aquarius level-2 official release product (V4.0), [*Meissner et al.*, 2014]; (2) Aquarius level-2 CAP product (V4.0), [*Yueh et al.*, 2014]; and (3) Aquarius level-3 Weekly polar-gridded product (V5.0), [*Brucker et al.*, 2014].

The ESA/SMOS satellite has only one sensor - a passive system called Microwave Imaging Radiometer using Aperture Synthesis (MIRAS) also operating at L-band. It has a tilt angle of 32.5° and spatial resolution of 35 km at center of field of view. The range of incidence angles varies from 0 to about 40 degrees over the field-of-view and the resolution changes with the angle of incidence. Total global coverage is achieved by SMOS in three days while the entire study domain is covered every two days. The mission required accuracy is 0.1 psu when data is averaged over a month on a 200-km scale [*Berger et al.*, 2002]. For this study, the Barcelona Expert Centre (BEC) SMOS level-3 Experimental product at high latitude ocean areas was used [*Gabarro et al.*, 2016]

Although they have the same goal of monitoring SSS using L-band observations, SMOS and Aquarius differ in both instrument design and SSS derivation approach. Aquarius has both radiometer and scatterometer, which helps in correcting for sea surface roughness. SMOS spatial resolution is finer than Aquarius' and also has shorter time of revisit. *Dinnat et al*, [2014b] compared SMOS and Aquarius SSS and observed that SMOS SSS values are generally lower than Aquarius SSS, except in cold waters. They also pointed out the difference between the forward models used; ancillary data utilized as input to the model, and the calibration parameters. SMOS uses the *Klein and Swift* [1977], while Aquarius uses the *Meissner and Wentz* [2012] dielectric constant model. The ancillary SSS used by SMOS for the forward model is the World Ocean Atlas 2009, [*Boyer et al.*, 2009], while Aquarius uses the Hybrid Coordinate Ocean Model (HYCOM), [*Chassignet et al.*, 2007]. Calibration was also done over a region in the Pacific Ocean for SMOS while for Aquarius it is done globally. Details of the SSS gridded data products used in this study are presented in the following sections.

2.2.1. AqGSFC: Aquarius level-2 official release product (V4.0)

Produced by NASA Goddard Space Flight Center's Aquarius Data Processing System (ADPS), Aquarius level-2 product contains retrieved orbital/swath SSS, wind speed from both radiometers and scatterometer, brightness temperature at V and H polarization, quality flags, converted telemetry, navigation data and ancillary data from select sources. In this study, we use the latest version (V4.0) which provides estimates of density and SSS-uncertainty variables and have the SST-dependent bias correction implemented directly into the baseline algorithm. Significant wave height (SWH) for surface roughness correction was also included along with tuning of parameters of the RFI filter over land. More details on the improvements made from V3.0 to V4.0 are in the dataset validation analysis done by *Lagerloef et al.* [2015] and accompanying Addendum to the ATBD by *Meissner et al.* [2015]. Dataset and user guide were downloaded from NASA's Physical Oceanography Distributed Active Archive Center (PO.DAAC), ftp://podaac.jpl.nasa.gov/SalinityDensity/aquarius/.

In this study, the SSS gridded product called AqGSFC, was generated using the level-2 orbital/swath official release data. The data were first geophysically filtered in a given grid point by discarding retrieved salinity with land fraction greater than 0.01, sea ice concentration greater than 0.01 and wind speed greater than 20 m/s. Wind speed greater than 20 m/s causes surface roughness that requires a special correction. Data with the following contamination flags (and flag number) were also removed from the gridded product: unusual brightness temperature (flag #6); direct solar flux contamination (#7); reflected solar flux contamination (#8); sun glint (#21); non-nominal navigation (#12); pointing anomaly (#16); brightness temperature consistency (#17); RFI contamination (#19) and Moon and Galactic reflected contamination (#21). Salinity measurements more than 40 psu or less than 20 psu were not included. To further remove data points potentially contaminated by presence of sea ice, Bootstrap Sea Ice Concentration (SIC) data from the Special Sensor Microwave/Imager (SSM/I) and Special Sensor Microwave Imager/Sounder (SSMIS), also known as the SB2 product [*Comiso et al.*, 2017] was used to mask out SSS readings with SIC greater than 15%. This was performed as the existing ice fraction derived from Aquarius brightness temperature tends to overestimate sea ice fraction in the marginal ice zone [*Dinnat and Brucker,* 2017]. The ice edge as inferred from SSM/I has been validated to be reasonably accurate even during the meltponding season [Comiso and Nishio, 2008].

Both ascending and descending orbits from all three beams were used in the processing. Each beam was filtered to suppress the noise along track, which was earlier suggested by *Melnichenko et al.* [2014] as a necessary step to improve accuracy of individual measurements along the track. Figure 2 shows the three beams (dotted line) passing through North Atlantic (Ascending) and North Pacific (Descending) starting at 6:12 PM UTC on 02 July 2012. The solid curves in Figures 2a and 2b are the result after the initial geophysical filtering and subsequent smoothing with a median filter with window of 9 observations. Aquarius data block period is every 1.44 seconds. It can be seen that random short-wavelength noise along track per beam was effectively suppressed. Another issue is the differences between the three beams due to the slightly varied view of the ocean surface. Since the beams are with different incidence angles, the geophysical errors to be observed per beam are expected to be different [*Lagerloef et al.,* 2013]. Along with the geophysical filtering performed in the initial phase of processing, taking into account only severe conditions, we also tried to minimize the effect of inter-beam biases by performing bilinear interpolation in between beams. Given that the Aquarius SSS data are spatially inhomogeneous, a median filter was used to remove noise while preserving edges and important details in the data. Median filter is also effective in removing random noise (isolated high or low values) and requires much less processing time than removal by frequency domain Fourier transforms

[*Nichols, et al.*, 2004]. Level-2 orbital/swath files were gridded on to the polar stereographic grid with 12.5 km resolution. This resolution was chosen because Aquarius has an along-track sampling of an observation every 10 km, thus, offering a refined spatial resolution. Running weekly maps were produced corresponding to the satellite's time of revisit for years 2011 to 2015. The location of the ice edge was also indicated by including a contour of the SB2 SIC edge in the SSS maps.

2.2.2. AqJPL: Aquarius Level-2 Combined Active-Passive (CAP) product (V4.0)

The level-2 CAP SSS and wind speed are calculated using the updated CAP retrieval algorithm [*Yueh et al.*, 2014] from Aquarius T_B and scatterometer backscatter by minimizing the sum of squared differences between model and observations. Aside from the CAP algorithm outputs, the product also includes flags for valid data and data with possible rain contamination using match-ups based on NOAA Climate Prediction Center morphing method (CMORPH) half-hourly global precipitation estimates at 0.25° resolution. It is distributed through NASA's Physical Oceanography Distributed Active Archive Center (PO.DAAC) 's homepage, ftp://podaac.jpl.nasa.gov/SalinityDensity/aquarius/.

The SSS product as described above and called AqJPL also has rain correction and was gridded in the same projection, spatial and temporal resolution, and filtering techniques as that with the AqGSFC product. Observations with CAP flags ≥ 3 or ≤ 9 and ≥ 13 were discarded. More details on the Level-2 CAP flags are provided in the Aquarius CAP Algorithm and Data User Guide V4.0 [*Yueh et al.*, 2015]. SSS retrievals with land and ice fraction greater than 0.01, flagged with non-nominal navigation, and pointing anomaly were not included. Salinity measurements more than 40 psu or less than 20 psu were also discarded

2.2.3. AqNSIDC: Aquarius Level-3 weekly polar-gridded product (V5.0)

Level-3 weekly polar-gridded product (V5.0) by *Brucker, et al.* [2014], distributed by the US National Snow and Ice Data Center at http://nsidc.org/data/aquarius/index.html) was also processed from level-2 orbital/swath product and includes SSS at latitudes higher than 50°. Data set consists of the average SSS retrieved from all three Aquarius radiometers, gridded to the EASE2.0 grid with 36 km resolution. Interpolation was done using Delaunay triangulation. In this paper, for ease of comparison, this product, referred to as AqNSIDC, was regridded in the polar stereographic grid at 12.5 km resolution. Same smoothing technique was also applied as those used for the AqGSFC and AqJPL.

2.2.4. SmosBEC: SMOS-BEC Experimental product in high latitude ocean areas

Distributed by the Barcelona Expert Center (BEC) at http://cp34-bec.cmima.csic.es., the objectively analyzed high latitude SMOS SSS product was gridded on to the EASE grid at 25km resolution, averaged every nine days. The data, referred to as SmosBEC, is available for years 2011 to 2013 only. BEC processed the SMOS level-2 data by discarding salinity measurements with galactic, sun glint and surface roughness contamination. For this experimental product, BEC used the *Meissner and Wentz* dielectric constant model in the computation of SSS. The individual SSS measurements were subtracted from the computed SMOS climatological value to get an anomaly product. Annual objectively analyzed SSS climatological field (WOA13 V2.0) was added to the SMOS anomaly product to compute for the absolute value of SSS.

3. Comparative Studies and Error Analysis

Salinity data obtained from a research vessel and quality-controlled CORA (COriolis Ocean database for ReAnalysis) in situ dataset provided the key validation measurements used for comparative studies and for estimating the accuracy of satellite SSS data. A number of validation studies were conducted previously but done mostly in low latitude warm waters. For example, *Ebuchi* and *Abe* [2014] made use of Argo data in tropical areas and found a systematic negative bias in the satellite measurements, which they attributed to near-surface salinity stratification due to precipitation. Validation of Aquarius SSS data with moored buoys and Argo floats were also done by Tang, *et al.* [2014] and determined that between 40°S and 40°N there is a strong agreement between monthly Aquarius SSS and Argo measurements, except in the Eastern Pacific Fresh Pool and Amazon River outflow. Similarly, *Boutin et al.* [2013] showed that SMOS SSS agree well with Argo measurements with standard deviations of 0.35 in the Tropical Pacific Ocean and 0.28 in the Subtropical Atlantic Ocean and that the values correlate well with the freshening associated with precipitation as derived from SSMI rain in the Intertropical Convergence Zone of the Pacific. Also, *Banks et al.* [2012] found that the SMOS SSS products generally agree with Argo floats and ocean model simulations in the Atlantic Ocean except in coastal regions.

Despite the importance of having good SSS satellite retrievals at high latitudes, only a few SSS validation studies have been conducted so far in the region. The aforementioned decrease in SSS sensitivity with decreasing sea surface temperature (SST) has been reported by *Lagerloef et al.* [2015] but the overall quality of SSS in the Arctic has not been assessed. Also, significant instrument noise and large-scale satellite biases have been observed in the region [*Melnichenko et al.*, 2014]. In connection to this, *Kohler et al.* [2014] studied SST-related biases in both Aquarius and SMOS SSS products through their validation in the northern North Atlantic using ship-based TSG and Argo data. *Brucker et al.,* [2014] and *Dinnat and Brucker,* [2017] indicated that a key source of error in the retrieval of SSS from Aquarius in the polar oceans has been land and sea ice contaminations. Sea ice and land masks derived from satellite data are available to minimize this problem but the implementation of these masks by the different SSS products is different. Other potential sources of error are the uncertainty on SST and the sea water dielectric constant model [*Dinnat et al.*, 2014a].

3.1. Comparison with Thermosalinograph Data from Icebreakers

Collected in situ salinity data from PFS Polarstern with cruise IDs: ARK27-1, ARK27-2, and ARK27-3 from 15 June to 06 October, 2012 and ANT28-3, ANT28-4, and ANT28-5 from 08 June to 04 October, 2014, covering Nordic Seas and the Arctic Ocean were used to validate the satellite-derived gridded SSS products. Only TSG measurements with quality flag equal to 1 (good) were used for this study. However, there is a possibility that the TSG measurement might represent a perturbed version of the surface that might cause mismatches with the satellite measurements. Figure 3 shows color-coded tracks of the ship to indicate salinity values observed along the tracks and location of comparative studies. The contour of the SB2 sea ice concentration product during each year's minima was also applied to indicate the location of the sea ice edge. Two sensors installed in the ship's bow and keel measured salinity of the seawater. Both are regularly calibrated with accuracy of <0.01. Data were downloaded from http://cdiac.ornl.gov/ftp/oceans/VOS_Polarstern/.

It is clearly seen in Figure 3 that the spatial distribution of the ship SSS measurements appears to be generally consistent with the presence of low surface salinities in the Arctic Ocean and bordering seas, likely associated with the melt of sea ice and river run-off during the June to October period for both 2012 and 2014.

Direct comparison of Polarstern SSS and the different satellite derived SSS products as discussed earlier are presented in Figure 4a to 4d. The plots are color-coded to show differences in the SSS values for different time periods and locations during the 2012 campaign as indicated as transect A to D in Figure 3a. The in situ Polarstern data have much larger spatio-temporal variability than the remote sensing products in part because the sampling is much more frequent than those of the satellite data sets (e.g. sampled every minute compared to multi-day averages) and the satellite sensor footprints are much larger than single point ship observations. Aquarius has three ellipsoidal footprints of 74 km x 94 km, 84 km x 120 km, and 96 km x 156 km, while SMOS has a footprint of 40 km. The discrepancies between the different products are sometimes quite large and in some places greater than 1 psu with SmosBEC appearing to be the one most consistent with Polarstern except in Figure 4b, where the ship measured SSS as low as 25 psu, which were effectively captured by the Aquarius products. The values usually fall between 34 and 36 psu, except in Figure 4b where the salinities are much lower and between 25 to 32 psu as expected in the Central Arctic during this time period because of the melt of sea ice and river runoffs.

Scatter plots showing more direct comparison of the different satellite products with Polarstern data are presented in Figure 4e to 4h. The results are similar for the different products with the

AqGSFC having the lowest standard deviation of 0.47 psu while AqJPL has the highest at 0.55 psu. Also, SmosBEC has the lowest RMS error of 0.51 psu while AqNSIDC has the highest at 0.69 psu. The correlation coefficients are all high, averaging 0.97, indicating good general agreement of satellite with in situ data.

The AqNSIDC product [*Brucker et al., 2014*] has larger RMS error in part because it allows for larger sea ice fractions in the product, which also keeps lower SSS values in the maps (down to ~ 25 psu). It is a compromise between letting the error grow and removing some features near the ice edge. The product was designed this way to let the user apply their best judgment for the given application; here all available values were used.

Similar plots but for data in 2014 are presented in Figure 5. SmosBEC data has not been processed for 2014 and later years and therefore missing in the comparative study. The plots show that Polarstern data agree best with AqNSIDC in Transect E (Figure 5a) while they agree best with AqGSFC and AqJPL in Transect F (Figure 5b). In Figure 5c, AqGSFC and some AqNSIDC measurements were able to follow the low salinity readings of the ship, with SSS ranging from 33 to 25 psu measured in the Arctic Ocean at the end of summer and early autumn (see Figure 3b). AqJPL did not have SSS data on this segment perhaps because of inaccurate masking of sea ice as well as the stringent parameters used in the CAP flags relative to wind speed and possible rain contamination. In addition, AqGSFC and AqJPL appear to be more consistent with each other. The large difference between the AqNSIDC with the other Aquarius products is unexpected and could be attributed to the along-track filtering performed on AqGSFC and AqJPL to get rid of random short-wavelength noise per beam. AqNSIDC product is also available as a weekly average and not on a running weekly average, which can slightly affect the accuracy of each collocation, centered on the ship's observation date.

Although the scatter plots show general agreement with high correlations, some biases are still observed and can also be a result of short time scale surface mixing as indicated earlier or other processes. Table 1 summarizes the computed average biases, RMS errors and correlation coefficient values for years 2012 and 2014.

3.2. Comparison with CORA v5.0.

Another source of in situ data that can be used for validation studies is the Coriolis Ocean Dataset for Reanalysis Dataset (CORA). The latest publicly available version of the product is called CORA5.0, which provides a collection of existing in situ measurements of salinity on a global scale to up to year 2015. The data are aggregated from different instruments such as Argo floats, XBT, CTD, XCTD, French RV TSG measurements, Sea Mammals, Surface Drifters and Moorings, and are received and stored in the Coriolis database in collaboration with the In Situ Thematic Centre of the Copernicus Marine Service (CMEMS INSTAC). CORA measurements undergo various quality checks and objective analysis to guarantee spatial and temporal consistency. Detailed information on the product is available at: http://marine.copernicus.eu/documents/PUM/CMEMS-INS-PUM-013-001-b.pdf. Data can be downloaded at: http://www.seanoe.org/data/00351/46219/.

In this study, geographically and daily surface data, starting 26 August 2011 to 06 June 2015 with quality index 1 – 4 (good to acceptable) were used and mapped to the same grid format as in the other data sets. The data accumulated for said dates are presented in Figure 6a and it is apparent that the data coverage is relatively sparse. However, the spatial distribution of SSS as depicted appears to be generally consistent with satellite data. For quantitative comparison with the satellite SSS products, scatter plots of CORA5.0 SSS data versus those of the four products are shown in Figures 6b, 6c, 6d and 6e. The scatter plots show relatively good agreement in most points in all products. Regression analysis was done on each set of products with CORA5.0 (blue) and on datasets common among all the products with CORA5.0 (red) to remove the impact of the differences in coverage between the products. Outliers are also filtered out. It is interesting to note that there are two distinct clusters, especially when considering data common among products, with the upper one corresponding to the data measured from the Atlantic and the lower one for data in the Pacific. The clusters indicate that the two oceans are in different salinity regimes with the range of values indicated in the clusters. When all data available for each product are used, the correlation coefficients are 0.913, 0.906, 0.898, and 0.944 for AqGSFC, AqJPL, AqNSIDC and SmosBEC, respectively. When only data points common to all four satellite products are used, the corresponding values are 0.921, 0.920, 0.898 and 0.943. This shows that the lower correlation coefficient of Aquarius products in the first set, in particular for AqNSIDC, is in part due to more data being available in challenging areas such as near land and ice. The RMS errors considering all common measurements are 0.412, 0.487, 0.465 and 0.323, which are much better that those derived from the comparative analysis using Polarstern data. The actual error in the satellite data is likely smaller since the CORA5.0 data set is not perfect as indicated above and there are uncertainties in the matching of in situ with satellite data. Overall, the results indicate that the data is promising with the correlation coefficients being quite high and the RMS errors relatively low.

4. Results of Analysis

4.1 Comparison of Spatial Distribution for Different SSS Products

Typical SSS distributions in the Arctic region as derived from the different products during spring and early autumn are presented in Figures 7 and 8. Figures 7a through 7d shows weekly averages for the period 31 May to 6 June using AqGSFC and AqJPL data and the period 31 May to 7 June for AqNSIDC and 31 May to 7 June for SmosBEC data. For convenience in the comparative analysis, the different products are mapped in the same format and covering the same general area. Note that the high latitude AqNSIDC and SmosBEC products cover greater than 50°N and 45°N only, respectively, while the AqGSFC and AqJPL products which are both derived from level 2 products provide data for the entire mapping region. In the comparative analysis, we show differences between data sets where there is overlapping data. The slight differences in dates are caused by differences in the dates of the original products but should be a minor issue in the qualitative comparison.

The spatial distribution of the different products shows similar general characteristics. For example, the salinities in the Northern Pacific Ocean are generally lower than those in the Northern Atlantic Ocean as mentioned earlier. This is consistent with more precipitation than evaporation in the Pacific Ocean and vice versa in the Atlantic Ocean [*Broecker, 1997*]. Also, salinities at lower latitudes are generally higher than those at higher latitudes. The salinity distributions are most similar for AqGSFC and AqJPL as would be expected since they are derived from the same level 2 Aquarius data set but with different retrieval algorithms. AqNSIDC (Figure 7c) shows the smoothened version of the product, which effectively removed the striped noise caused by the push-broom configuration of the Aquarius sensor as well as minimized the effect of the unique sampling pattern of Aquarius satellite, where two or even three beams coincide [*Lilly et al.*,2008]. Figure 7d shows basically the same pattern as the other three Aquarius products but the SmosBEC product seems to display more noticeable differences especially in the Bering Sea and freshening close to the mouth of Amur River in the Okhotsk Sea. The differences are better quantified in Figures 7e, 7f, 7g and 7h, with the largest discrepancies observed in the seasonal ice region (e.g., Okhotsk Sea) and likely associated with the presence of sea ice.

The maps presented in Figure 8 are similar to those in Figure 7 but for the end of the summer to early autumn and early autumn when the sea ice cover usually reaches its minimum. It is the time period when the Arctic Basin has the least ice cover and more open water areas exposed to satellite salinity measurements. Again, the maps shown in Figures 8a, 8b and 8c are generally consistent but the coverage differs depending on the way the sea ice cover is masked from the data. In this case AqNSIDC shows the least ice-related gaps due to the higher threshold of the mask (Fig. 8c) while AqJPL shows more gaps than actually depicted in ice maps measured by passive microwave sensors (i.e., see ice edge indicated by the red contour). All data products show significantly lower salinity inside the Arctic basin than other areas. SmosBEC data show the relatively low salinity close to river mouths as expected due to river runoff but little coverage in the Arctic Basin because of poor sea ice masking (see Figure 8d). The difference maps presented in Figures 8e to 8f shows a generally higher SSS in the AqJPL than the AqGSFC and AqNSIDC products. The SmosBEC shows comparable but mainly lower values than AqGSFC except in the

South Atlantic Ocean region. Some anomalously high discrepancies are apparent in the Arctic Basin that are likely mainly associated with contamination of the data by sea ice.

As previously observed in the SSS maps during spring, SmosBEC (Figure 8g and 8h) retrieved more pronounced SSS variations close to the mouth of major Arctic rivers emptying into the Arctic basin. The plume of Amur River (see Figure 1) flowing to the Sea of Okhotsk, measures up to 2-3 psu lower than that of both AqGSFC and AqJPL. By the end of summer, lower SSS in the river plumes of Kolyma, Ob and Mackenzie rivers can also be observed in the SmosBEC map. However, AqGSFC, AqJPL and AqNSIDC showed more pronounced freshening in Beaufort Sea as well as close to the mouth of Lena River, emptying into Laptev Sea. This supports the validation findings using ship data, (as shown in Figures 4b and 4h) where SmosBEC got higher SSS measurements (~3-4 psu) when compared to ship TSG measurements. In addition, AqNSIDC and SmosBEC (other products not available) differ significantly in their depiction of the Kara Sea river plume at the early autumn of 2012. SmosBEC shows a central propagation while AqNSIDC shows an Eastern propagation, with the plume being pressed toward the Siberian coast. Analysis by *Kubryakov et al.* [2016] suggests that in 2012 the river plume was propagating eastward. The SmosBEC pattern may have been distorted by the calibration to the climatology, the Eastern propagation of the plume being an unusual occurrence.

In the Atlantic Ocean region, Aquarius products as compared to the SmosBEC product best captured the freshening caused by the melting of sea ice along the coasts of Greenland as well as the melt of glaciers and the Greenland ice sheet *[Khan et al, 2014; Dukhovskoy et al, 2016]*. The flow of fresh water from Davis Strait and Labrador Sea to the North Atlantic Ocean is also shown to be pronounced in the Aquarius products in the early autumn. The export of low salinity polar water to the North Atlantic is expected to affect the freshwater balance in the Arctic Ocean and can have significant impact on the global climate *[Rudels,* 2011]. In comparing AqJPL and AqGSFC, it can be seen that in general, AqJPL measured relatively higher salinity in early autumn and relatively lower in spring.

4.2. Interannual Variations in Salinity Distributions During Spring and Early Autumn

The interannual changes in sea surface salinity have been quantified for the time period Aquarius SSS data are available. Interannual changes are important to monitor because reports indicate that SSS has been getting saltier in the Northern Atlantic while it is getting fresher in the Northern Pacific *[Gordon and Giulivi, 2008]*. Salinity maps for spring and early autumn are presented in Figures 9 and 10, respectively. The spatial distribution of salinity in spring as described for 2012 in the previous section is also true for the other years as depicted in Figure 9. The yearly differences are mainly in the seasonal regions and are most apparent in AqGSFC and AqJPL since these maps show data at lower latitudes. The changes are most evident in the Pacific Ocean where the 33 psu contour (in black) shows significant interannual variability. Note that the patterns of interannual changes from the different products are similar despite significant differences of the different products and especially those for AqGSFC and AqJPL which covers the entire study areas. The observed interannual changes are likely associated with interannual changes in ice cover, ice dynamics and precipitation as maybe influenced by ENSO and the Pacific Decadal Oscillation. Since the differences between the four products are due to different processing and noise reduction techniques the latter can be made more uniform to minimize the differences. Subtler changes in SSS are observed in the Atlantic Ocean.

In early autumn, Figure 10 shows that interannual changes are apparent in all four products. In the Pacific Ocean, significant interannual changes are evident especially in the Bering Sea and the Okhotsk Sea. For example, SSS in parts of the Bering Sea in 2011 is almost 1 psu lower than the SSS in 2014 in the three Aquarius products. Also, SSS in the Okhotsk Sea is lower in 2013 than those of the other years. In the Arctic basin, the interannual differences are mainly due to yearly change in the Arctic sea ice cover. Large differences in the masking of the sea ice cover (and also land) are apparent for the different products making salinity data from these products less uniform in the Arctic basin.

The changes in Kara Sea's plume distribution, particularly its westward extension was shown to vary from year to year depending on wind regime [*Kubryakov et al.*, 2016]. This can be observed in the AqNSIDC and SmosBEC products due to their extended coverage, which included more data closer to the coast. SmosBEC shows changes in the extent of fresh water from the rivers plume, while AqNSIDC shows changes both in extent and in shape of the plume. A possible salt water intrusions from the Pacific Ocean through the Bering strait is also apparent in the Aquarius products where some elevated SSS values at the Chukchi Sea are depicted. Such phenomenon has been reported previously by [Coachman and Barnes, 1961]. The intruding Bering Sea water separates deeper Atlantic water from the surface water in the Arctic and limits the depth of vertical convection associated with the freezing of ice.

The results of quantitative assessment of the differences of the various products are presented in Figure 11. Figures 11a and 11b shows monthly changes in salinity from 2011 through 2015 for the Northern Pacific and Northern Atlantic Oceans areas, respectively. In the Northern Pacific Ocean there appears to be a general agreement with the AqGSFC showing the most consistent seasonality while SmosBEC shows the least seasonality and most discrepancy from the others. This is possibly due to the use of climatological data to debias the SMOS retrievals. In the Northern Atlantic Ocean, the discrepancies between the products are more significant and biases between the different Aquarius products are more apparent.

Figures 11c and 11d show plots of SSS data > 65°N in both Western and Eastern Arctic Basin. It is remarkable that the four SSS products agree so well in the region. In the Western Arctic Basin, there is a good general agreement in the average values > 65°N with the monthly and interannual changes associated with the changes in the sea ice cover. For convenience, the sea ice concentration is plotted as a dash line to be able to assess the effect of sea ice melt. The lowest average salinity values are indeed observed in early autumn 2012 when the extent of sea ice was a record low and significant areas of open water are exposed. However, in Figure 11c, SmosBEC show significantly higher SSS during the early autumn of 2012 than the other three products. Improper masking of the sea ice cover as can be seen in Figure 10 causes this. In Figure 11d, the AqJPL data does not show the drop in SSS during the early autumn of 2014. Again, this is caused by improper masking of sea ice in the Arctic Basin. The good agreement of the three products does not necessarily indicate good accuracy since the Arctic Basin is an area where the uncertainties in the retrieval is supposed to be greater because of colder temperatures. There could be a bias in the retrieved data that is currently not easy to detect due to the paucity of in situ observations.

5. Discussion and Conclusions

The spatial and temporal distributions of SSS at high latitudes are studied through comparative analysis of four different surface salinity products derived from L-band observations and ancillary data. The four products include three from Aquarius as processed by different groups and one from SMOS. The accuracy of each product is assessed through regression and correlation analysis with quality-controlled ship measurements and CORA5.0 data set. The RMS errors when compared with CORA5.0 data are 0.412, 0.487, 0.465 and 0.323 psu for the AqGSFC, AqJPL, AqNSIDC and SmosBEC products, respectively. The RMS errors are very similar with SmosBEC having a slight advantage in accuracy. The actual accuracy could be better since the CORA5.0 data used in the analysis are not perfect and there are also errors in the matching of the in-situ with the satellite products (e.g., footprint and ocean depth). Also, it is important to note that the instruments were built to have a precision of about 0.2 psu. The RMS errors using ship/Polarstern data in the Arctic region are higher at 0.515, 0.585, 0.686 and 0.507 psu for the AqGSFC, AqJPL, AqNSIDC and SmosBEC products in 2012 and 0.806, 0.838, and 0.886 psu for AqGSFC, AqJPL and AqNSIDC in 2014. The higher RMS errors when using ship data are likely associated in part with the difficulty of matching ship measurements with satellite measurements. The SmosBEC product is again more consistent than the other products in 2012 with RMS error of 0.507 psu but only slightly with the value of AqGSFC being very similar at 0.515 psu. The difference is in part due to a bias correction using climatological data was applied in the computation of SmosBEC product.

It should be noted that there are significant differences even between the three Aquarius SSS products. The differences are usually caused by different techniques in the retrieval of SSS.

Even when the retrieval techniques are the same such as those used in the AqGSFC and AqNSIDC products, there are still biases associated with the geophysical filtering and smoothing techniques. In addition, the masking of sea ice and land are different for the different products. For example, inability to mask sea ice cover properly keeps the AqJPL data from capturing the seasonal variability in SSS that is observed by AqGSFC and AqNSIDC products in the Arctic region in the early autumn of 2014. Also, although SmosBEC provides SSS that is most consistent with ship and CORA5.0 data, the masking of sea ice was not done properly in the retrieval. This limit the usefulness of this (and also JPL) product in the Arctic basin and points to the need to validate or improve the ice concentration product used to mask out sea ice contaminated SSS.

Overall, all four products are highly correlated with CORA5.0 and ship data and the spatial and temporal changes in distributions are consistent with changing surface salinity associated with river run-off, sea ice and glacial melt and exchanges between the Arctic and the Pacific and Atlantic Oceans. The products can therefore be used to gain understanding of changing productivity in the region as may be associated with low salinity and phytoplankton blooms and near the ice edges and changes in the circulation patterns of the ocean. The results also show quantitatively that the Atlantic/Eastern side is consistently more saline than the Pacific/Western side for all seasons which opens up some questions about differences in precipitation patterns and mixing dynamics in the two oceans.

Acknowledgements

We are grateful to the NASA Cryospheric Sciences Program for providing funding support for this project (Grant 444491.02.01.02.76). We also thank Robert Gersten of Wyle Inc. and Larry Stock of SGT Inc. for programming support. The SSS satellite products, namely Aquarius weekly polar-gridded product was provided by the National Snow and Ice Data Center (NSIDC), Aquarius level 2 and Aquarius level 2 CAP from the NASA Physical Oceanography Distributed Active Archive Center (PO.DAAC) at the Jet Propulsion Laboratory, and the SMOS High Latitude product from the Barcelona Expert Centre (BEC). The quality-controlled in situ TSG SSS data was obtained from the Carbon Dioxide Information Analysis Center (CDIAC) report under VOS_Polarstern for 2012 and 2014 while CORA version 5.0. from the Copernicus Marine Environment Monitoring Service (CMEMS). The gridded weekly (or 8-day) averages of SSS data, referred to in the manuscript as AqGSFC, AqJPL, AqNSIDC and SmosBEC, can be downloaded from the following GSFC website: https://www.neptune.gsfc.nasa.gov.

References

Aagard, K., and E.C., Carmack, J.H. Swift (1985), Thermohaline Circulation in the Arctic Mediterranean Seas, *Journal of Geophysical Research*, Vol. 90, No. C3., pp. 4833-4846.

Banks, C. J., C. P. Gommenginger, M. A. Srokosz, H. M. Snaith (2012), Validating SMOS Ocean Surface Salinity in the Atlantic with Argo and Operational Ocean Model Data, *IEEE Transactions on Geoscience and Remote Sensing*, 50. pp.1688-1702, doi: 10.1109/tgrs.2011.2167340.

Berger M., A. Camps, J. Font, Y. Kerr, J. Miller, J. Johannessen, J. Boutin, M. R. Drinkwater, N. Skou, N. Floury, M. Rast, H. Rebhan, and E. Attema, (August 2002), *Measuring Ocean Salinity with ESA's SMOS Mission – Advancing the Science*, ESA Bulletin 111.

Boutin, J., N. Martin, G. Reverdin, X. Yin, and F. Gaillard (2013), Sea surface freshening inferred from SMOS and ARGO salinity: impact of rain, *Ocean Science*. 9. pp. 183-192, doi: 10.5194/os-9-183-2013.

Boyer, T.P., J. I. Antonov, O. K. Baranova, H. E. Garcia, D. R. Johnson, R. A. Locarnini, A. V. Mishonov, D. Seidov, I. V. Smolyar, and M. M. Zweng (2009), *World Ocean Database 2009, Chapter 1: Introduction*, *NOAA Atlas NESDIS 66*, Ed. S. Levitus, U.S. Gov. Printing Office, Wash., D.C., 216 pp.

Broecker, W. S. (1997), Thermohaline circulation, the Achilles heel of our climate system: Will man-made CO2 upset the current balance?, Science, 278, 1582-1588.

Brucker, L., E. P. Dinnat, and L. S. Koenig (2014), Weekly gridded Aquarius L-band radiometer/scatterometer observations and salinity retrievals over the polar regions – Part 1: Product description, *The Cryosphere*, 8, pp. 905-913.

Brucker, L., E. P. Dinnat, and L. S. Koenig (2014), Weekly gridded Aquarius L-band radiometer/scatterometer observations and salinity retrievals over the polar regions – Part 2: Initial product analysis, *The Cryosphere*, 8, pp. 915-930.

Cabanes, C., A. Grouazel, K. von Schuckmann, M. Hamon, V. Turpin, C. Coatanoan, F. Paris, S. Guinehut, C. Boone, N. Ferry, C. de Boyer Montégut, T. Carval, G. Reverdin, S. Pouliquen, and P. Y. Le Traon (2013), The CORA dataset: validation and diagnostics of in-situ ocean temperature and salinity measurements. *Ocean Science*, 9, 1-18, http://www.oceansci.net/9/1/2013/os-9-1-2013.html, doi:10.5194/os-9-1-2013

Cavalieri, D. J. and C.L. Parkinson (2012), Arctic sea ice variability and trends, 1979–2010, *The Cryosphere*, 6, 881-889, doi:10.5194/tc-6-881-2012.

Chassignet, E.P., H.E. Hurlburt, O.M. Smedstad, G.R. Halliwell, P.J. Hogan, A.J. Wallcraft, R.

Baraille, R. Bleck (March 2007), The HYCOM (HYbrid Coordinate Ocean Model) data assimilative system, *Journal of Marine Systems*, vol. 65, Issues 1–4, pp. 60-83,

Coachman, L.K. and C.A. Barnes. (1961) The Contribution of Bering Sea Water to the Arctic Ocean. *Arctic*, Vol.14, No. 3. DOI: 10.14430/arctic3670

Comiso, J.C., R.A. Gersten, L.V. Stock, J. Turner, G.J. Perez, and K. Cho (2017), Positive Trend in the Antarctic Sea Ice Cover and Associated Changes in Surface Temperature. *J. Climate*, 30, 2251–2267, doi: 10.1175/JCLI-D-16-0408.1.

Comiso, J. C., C. L. Parkinson, R. Gersten, and L. Stock (2008), Accelerated decline in the Arctic sea ice cover, *Geophys. Res. Lett.*, 35, L01703, doi:10.1029/2007GL031972.

Gabarro C., E. Olmedo, A. Turiel, J. Ballabrera-Poy, J. Martinez, M. Portabella (2016), SMOS sea surface salinity maps of the Arctic Ocean, *EGU General Assembly 2016*, Geophysical Research Abstracts Vol. 18, EGU2016-7359-3

Dinnat, E. P., and D. M. Le Vine (2008), Impact of sun glint on salinity remote sensing: An example with the Aquarius radiometer, *IEEE Trans. Geosci. Remote Sens.*, 46(10), 3137–3150, doi:10.1109/TGRS.2008.2000629.

Dinnat, E. P., S. Abraham, D. M. Le Vine, P. De Matthaeis, and D. Jacob (2009), Effect of emission from the moon on remote sensing of sea surface salinity: An example with the Aquarius radiometer, *IEEE Geosci. Remote Sens. Lett.*, 6(2), 239–243, doi:10.1109/LGRS.2008.2008822.

Dinnat, E., L. Brucker (2017), Improved Sea Ice Fraction Characterization for L-band Observations by the Aquarius Radiometers, *IEEE Transactions on Geoscience and Remote Sensing*, 0196-2892

Dinnat, E., L. Brucker, I. C. Alvarez (2014a), Assessment of the Aquarius Space-borne Sea Surface Salinity Retrievals in Polar Oceans, *American Geophysical Union, Fall Meeting 2014*, Abstract #OS41C-1218.

Dinnat, E., J. Boutin, X. Yin, and D. Le Vine (2014b), Inter-comparison of SMOS and Aquarius sea surface salinity: Effects of the dielectric constant and vicarious calibration. *In: Microwave Radiometry and Remote Sensing of the Environment (MicroRad), 13th Specialist Meeting*; pp. 55-60. doi: 10.1109/MicroRad.2014.6878907.

Dukhovskoy, D. S., et al. (2016), Greenland freshwater pathways in the sub-Arctic Seas from model experiments with passive tracers, J. Geophys. Res. Oceans, 121, 877–907, doi:10.1002/2015JC011290.

Durack, P. J., S. E. Wijffels, and R. J. Matear (2012), Ocean salinities reveal strong global water cycle intensification during 1950 to 2000, *Science 336*, pp. 445-458.

Ebuchi, N., and H. Abe (2014), Evaluation of sea surface salinity observed by Aquarius, 2014 *IEEE Geoscience and Remote Sensing Symposium*, Quebec City, QC, pp. 4427-4430. doi: 10.1109/IGARSS.2014.6947473.

Gordon, A.L., and C.F. Giulivi. (2008) Sea Surface Salinity Trends: Over Fifty Years Within the Subtropical North Atlantic, *Oceanography*, Vol. 21, No.1. pp. 21-29, March 2008.

Houssais, M.N., C. Herbaut, P. Schlichtholz, C. Rousset. (2007) Arctic Salinity Anomalies and their Link to the North Atlantic during a Positive Phase of the Arctic Oscillation. *ScienceDirect, Progress in Oceanography*, 73 (2007) 160-189. DOI: 10.1016/j.pocean.2007.02.005

Khan, S. A., et al. (2014), Sustained mass loss of the northeast Greenland ice sheet triggered by regional warming, *Nat. Clim. Change*, **4**(4), 292–299, doi:10.1038/nclimate2161.

Kerr, Y., Waldteufel, J. P., Boutin, M. J. Escorihuela, J. Font, N. Reul, ... S. Mecklenburg (2010), The SMOS mission: New tool for monitoring key elements of the global water cycle, *Proceedings of the IEEE,* 98 (5), pp. 666-687.

Klein, L.A. and C. T. Swift (1977), An improved model for the dielectric constant of seawater at microwave frequencies, *IEEE Transactions on Antennas and Propagation*, vol. AP-25, no. 1, pp. 104–111.

Kohler J., M. S. Martins, N. Serra, D. Stammer (2014), Quality Assessment of spaceborne sea surface salinity observations over the northern North Atlantic, *Journal of Geophysical Research: Oceans*, 120, pp. 94-112. doi: 10.1002/2014JC010067.

Kubryakov, A., S. Stanichny, and A. Zatsepin (2016), River plume dynamics in the Kara Sea from altimetry-based lagrangian model, satellite salinity and chlorophyll data, *Remote Sens. Environ.*, 176, 177–187, doi:10.1016/j.rse.2016.01.020.

Lagerloef, G., F. R. Colomb, D. L. Vine, F. Wentz, S. Yueh, C. Ruf, ... C. Swift (2008), The Aquarius/SAC-D mission: Designed to meet the salinity remote-sensing challenge, *Oceanography*, 21(1), pp. 68-81.

Lagerloef, G., H. Y. Kao, T. Meissner, J. Vazquez (2015), *Aquarius Salinity Validation Analysis; Data Version 4.0. 2*. Available online at ftp://podaac-ftp.jpl.nasa.gov. Accessed: 26 Aug 2016.

Lagerloef, G., Kao, H.Y., Meln, O., Hacker, P., Hackert, E., Chao, Y., Hilburn, K., Meissner, T., Yueh, S., Hong, L., and Lee, T. (2013), *Aquarius Validation Analysis Technical Report*, AQ-041-PS-0016, NASA, Pasadena, CA, USA.

Lehner, F., C. C. Raible, D. Hofer, and T. F. Stocker (2012), The freshwater balance of polar regions in transient simulations from 1500 to 2100 AD using a comprehensive coupled climate model, *Clim. Dyn.*, **39**(1-2), 347–363, doi:10.1007/s00382-011-1199-6.

Le Vine, D., G. Lagerloef, and S. Torrusio (2010), Aquarius and remote sensing of sea surface salinity from space, *Proc. IEEE*, 98(5), 688–703.

Le Vine, D. M., E. P. Dinnat, S. Abraham, P. De Matthaeis, and F. J. Wentz (2011), The Aquarius simulator and cold-sky calibration, *IEEE Trans. Geosci. Remote Sens*., 49(9), 3198–3210, doi:10.1109/TGRS.2011.2161481.

Le Vine, D. M., S. Abraham, C. Utku, and E. P. Dinnat (2013), Aquarius third stokes parameter measurements: Initial results, *IEEE Geosci. Remote Sens. Lett.*, 10(3), 520–524, doi:10.1109/LGRS.2012.2211994.

Lilly, J.M., and G. S. Lagerloef (January, 2008), *Aquarius Level 3 Processing Algorithm Theoretical Basis Document Version 0.9.* Available online at ftp://podaac-ftp.jpl.nasa.gov. Accessed: 26 Aug 2016.

Martin, A. C. H., J. Boutin, D. Hauser, and E. P. Dinnat (2014), Active-passive synergy for interpreting ocean L-band emissivity: Results from the CAROLS airborne campaigns, *J. Geophys. Res. Ocean.*, 119(8), 4940–4957, doi:10.1002/2014JC009890.

Mecklenburg, S., Drusch, M., Kerr, Y., Font, J., Martin-Niera, M., Delwart, S., ... Crapoicchio, R. (2012), ESA's soil moisture and ocean salinity mission: Mission performance and operations, *IEEE Transactions on Geoscience and Remote Sensing*, 50 (5), pp. 1354-1366.

Meissner, T., Wentz, F.J., and Scott, J. (2015), *Remote Sensing Systems SMAP [8day] Mean Sea Surface Salinity on 0.25 deg grid, Version 1.0. (BETA).* Remote Sensing Systems, Santa Rosa, CA., Available online at www.remss.com/missions/smap. Accessed: 16 Sept 2016.

Meissner, T. and Wentz, F. (2012), The emissivity of the ocean surface between 6 and 90 GHz over a large range of wind speeds and earth incidence angles, *IEEE Trans. Geosci. Remote Sensing*, vol. 50, no. 8, pp. 3004– 3026.

Meissner, T., F. J. Wentz, and L. Ricciardulli (2014), The emission and scattering of L-band microwave radiation from rough ocean surfaces and wind speed measurements from the Aquarius sensor, *J. Geophys. Res. Ocean*., 119(9), 6499–6522, doi:10.1002/2014JC009837.

Meissner, T., Wentz, F.J., and De Mattheis P. (July 15, 2015), *Addendum IV to ATBD, Remote Sensing Systems Report #071515*, Santa Rosa, CA., Available online at ftp://podaac-ftp.jpl.nasa.gov/allData/aquarius/docs/v4/AQ-014-PS-0017_AquariusATBD_Level2_Addendum4_DatasetVersion4.0.pdf. Accessed: 26 August 2016.

Melnichenko, O., Hacker, P., Maximenko, N., Lagerloef, G., and Potemra, J. (2014), Spatial Optimal Interpolation of Aquarius Sea Surface Salinity: Algorithms and Implementation in the North Atlantic, *Journal of Atmospheric and Oceanic Technology*, 31, pp. 1583-1600.

Nichols, J.E. and V. Vohra (2004), *Noise over water surfaces in Landsat TM images*, International Journal of Remote Sensing, 25 (11), pp. 2087 - 2093.

Nummelin, A., M. Ilicak, C. Li, and L. H. Smedsrud (2016), Consequences of future increased Arctic runoff on Arctic Ocean stratification, circulation, and sea ice cover, J. Geophys. Res. Oceans, 121, 617–637, doi:10.1002/2015JC011156.

Rudels, B., (2011) Volume and freshwater transports through the Canadian Arcgtic Archipelago-Baffin Bay system, J. Geophys. Res, 116, C00D10, doi:10.1029/2011JC007019.

Schmitt, R.W. (March 2008), Salinity and the Global Water Cycle, *Oceanography*, 21 (1). 12-19.

Serreze, M.C., Barrett, A.P., Slater, A.G., Woodgate, R.A., Aagaard, K., Lammers, R.B., Steele, M., Moritz, R., Meredith, M., and Lee, C.M. (2006), The large-scale freshwater cylce of the Arctic, *Journal of Geophysical Research*, 111, C11010. doi: 10.1029/2005JC003424.

Szekely, T., Gourrion, J., Brion, E., Von Schuckmann, K. Reverdin, G., Grouazel, A., and Pouliquel, S., 2015: CORA4.1: A delayed-time validated temperature and salinity profiles and timeseries product. Proceeding from 7e EuroGOOS conference, To be published.

Vaughan, D., J. Comiso, I.,Allison, J.Carrasco, G.Kaser, R.Kwok, P.Mote, T.Murray, F.Paul, J.Ren, E.Rignot, O.Solomina, K.Steffen, and T.Zhang (2013), *Observations: Cryosphere, in: Climate Change 2013: The Physical Science Basis. Contribution of Working Group I to the Fifth Assessment Report of the Intergovernmental Panel on Climate Change*, edited by: Stocker, T., Qin, D., Plattner, G.-K., Tignor, M., Allen, S., Boschung, J., Nauels, A., Xia, Y., Bex, V., and Midgley, P., Cambridge University Press, New York, NY, USA, 2014.

Wentz, F. J., and D. M. LeVine (2012), *Aquarius salinity retrieval algorithm version 2: Algorithm theoretical basis document*, RSS Tech. Rep. 082912, pp. 45. Available at ftp://podaac-ftp.jpl.nasa.gov/allData/aquarius/docs/v2/AQ-014-PS-0017_AquariusATBD_Level2. pdf. Accessed: 26 August 2016.

Wentz, F.J., and S. H. Yueh (August 16, 2011), *Algorithm Theoretical Basis Document (ATBD), Version 1*, Aquarius Salinity Retrieval Algorithm, RSS Tech Report 081611. Accessed: 26 August 2016.

Yueh, S. H., and J. Chaubell (2012), Sea Surface Salinity and Wind Retrieval Using Combined Passive and Active L-Band Microwave Observations, *Geosci. Remote Sensing, IEEE*

Trans., 50(4), 1022–1032, doi:10.1109/TGRS.2011.2165075.

Yueh, S. H., R. West, W. J. Wilson, F. K. Li, E. G. Njoku, and Y. Rahmat-Samii (2001), Error sources and feasibility for microwave remote sensing of ocean surface salinity, *IEEE Trans. Geosci. Remote Sens.*, 39(5), 1049–1060.

Yueh, S.H., S. J. Dinardo, G. Gore, and F. K. Li (2010), Passive and Active L-Band Microwave Observations and Modeling of Ocean Surface Winds, *IEEE Transactions on Geoscience and Remote Sensing*, 48(8), 3087-3100.

Yueh, S.H., W. Tang, A. Fore, and A. Hayashi (September 20, 2015), *Aquarius CAP Algorithm and Data User Guide version 4.0*, Available online at ftp://podaac-ftp.jpl.nasa.gov/allData/aquarius/docs/CAPv2/Aquarius-CAP-User-Guide-v2.0.pdf Accessed: 26 August 2016.

Yueh S.H., W. Tang, A. Fore, A. Hayashi, Y.T. Song, and G. Lagerloef (2014), Aquarius geophysical model function and combined active passive algorithm, for ocean surface salinity and wind retrieval, *Journal of Geophysical Research: Oceans*, 119, 5360-5379. doi:10.1002/2014JC009939.

Table 1. Comparison of space observed SSS products and Polarstern TSG measurements with the values averaged over all collocated measurements for 2012 and 2014. (SmosBEC product available only from 2011-2013).

	15 Jun - 06 Oct 2012				08 Jun – 04 Oct 2014		
	AqGSFC	AqJPL	AqNSIDC	SmosBEC	AqGSFC	AqJPL	AqNSIDC
Correlation	0.974	0.964	0.972	0.959	0.876	0.393	0.780
SD	0.467	0.547	0.524	0.486	0.569	0.408	0.691
Bias	0.117	-0.170	0.263	0.011	0.572	0.663	-0.555
RMSE	0.515	0.585	0.686	0.507	0.806	0.838	0.886

List of Captions:

Figure 1. Panel a shows location of in situ data from the CORA v5.0 for year 2012 as received by the Coriolis data Centre and illustrates the paucity of data in the Arctic region. Blue data points represent Argo data while the red points are from other sources (e.g., XBT, CTD, ship etc.). Also indicated are various seas in the region as well as the mouth of key rivers. Panels b-c illustrate dependence of T_B in the V and H polarizations to SST at different SSS ranging from 25-29 psu at 1.43 GHz frequency and 35° incidence angle.

Figure 2. Aquarius Level-2 SSS three beams (dotted line: Beam1-black; Beam2-red; Beam3-blue) passing through North Atlantic (Ascending) and North Pacific (Descending) starting at 6:12PM UTC on July 2, 2012. Solid line show result after applying median filter along track with window of 9 observations.

Figure 3. Polarstern track from (a) 15 June – 06 October 2012 and (b) 08 June – 04 October 2014, covering Norwegian Sea, Greenland Sea, Fram Strait, Arctic Ocean, Barents Sea and

Laptev Sea. Letters A-D in 2012 and E-G in 2014 are portions of the ship's tracks used for the validation of the satellite derived salinity measurements. Tick marks of varied shapes indicate extent of each segment used.

Figure 4. Comparison of Polarstern TSG measurements (black) versus collocated satellite-derived SSS products namely: AqGSFC (red), AqJPL (orange), AqNSIDC (blue), and SmosBEC (green) from 15 June – 06 October 2012. Areas (a-d) are segments of the ship tracks that are not contaminated by sea ice or land as illustrated in Figure 3. Scatter plots of co-located (a) AqGSFC; (b) AqJPL; (c) AqNSIDC; and (d) SmosBEC versus Polarstern TSG measurements for the same period.

Figure 5. Comparison of Polarstern TSG measurements (black) versus collocated satellite-derived SSS measurements from AqGSFC (red), AqJPL (orange), AqNSIDC (blue), and SmosBEC (green) from 08 June – 04 October 2014**.** Areas (a-d) were highlighted due to the absence of possible contamination from sea ice and land. Scatter plots of co-located (a) AqGSFC; (b) AqJPL; and (c) AqNSIDC versus Polarstern TSG measurements for the same period.

Figure 6. In situ SSS map from 26 August 2011 to 06 June 2015 using (a) CORA5.0 and scatter plots of collocated satellite-derived SSS data from (b) AqGSFC, (c) AqJPL, (d) AqNSIDC, and (e) SmosBEC versus CORA5.0. Scatterplots of each of the products with CORA5.0 are shown in blue while data points common among all the products with CORA5.0 are shown in red.

Figure 7. Difference map (e) shows the difference between processed (a) AqGSFC from (b) AqJPL; difference map (f) is the difference between (a) AqGSFC and (c) AqNSIDC; difference map (g) between (a) AqGSFC and (d) SmosBEC; and difference map (h) is the between (b) AqJPL and (d) SmosBEC all in the middle of spring of 2012.

Figure 8. Difference map (e) shows the difference between processed (a) AqGSFC from (b) AqJPL (b); difference map (f) is the difference between (a) AqGSFC and (c) AqNSIDC ; difference map (g) between (a) AqGSFC and (d) SmosBEC; and difference map (h) is the between (b) AqJPL and (d) SmosBEC all in the end of early autumn of 2012.

Figure 9. Inter-annual SSS distribution in spring of 2011-2015 from (a) AqGSFC, (b) AqJPL, (c) AqNSIDC and (d) SmosBEC product from 2012-2013. Also shown are 33 psu contours in black.

Figure 10. Inter-annual SSS distribution in early autumn 2011-2014 from (a) AqGSFC, (b) AqJPL, (c) AqNSIDC and (d) SmosBEC product from 2011-2013. Also shown are 33 psu contours in black.

Figure 11. Monthly SSS averages of AqGSFC (red), AqJPL (yellow), AqNSIDC (blue) from August 2011 to June 2015 and SmosBEC from August 2011 to December 2013 in the (a) Pacific Ocean (> 50°N, < 65°N, < 270°E, > 90°E), Atlantic Ocean (> 50°N, < 65°N, < 90°E, > 270°E), Western Arctic Basin (> 65°N, < 180°E, > 0°E), and Eastern Arctic Basin (> 65°N, > 180°W, > 0°W). SB2 sea ice concentration monthly averages plotted on c-d are shown as the gray dashed line.

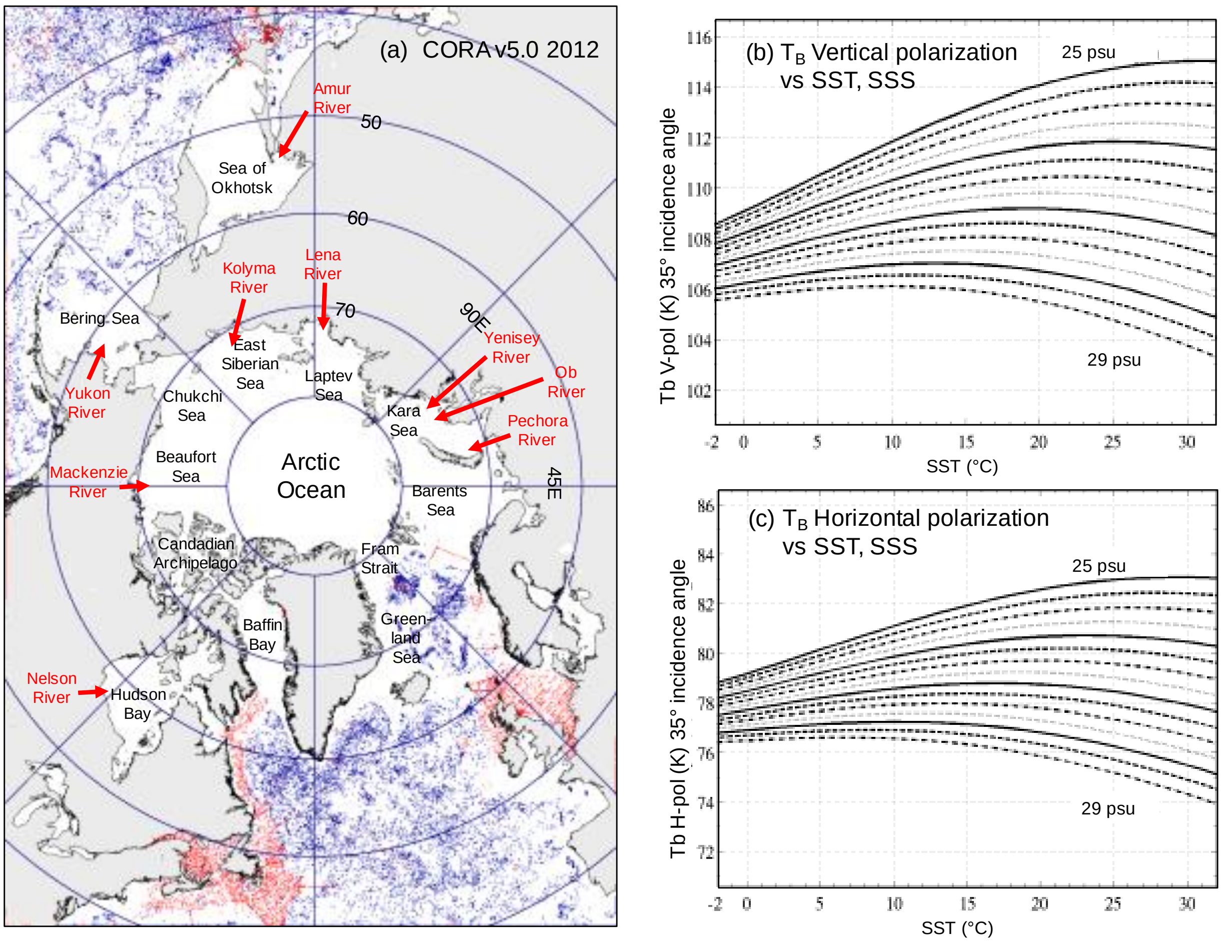

Figure 1. Panel a shows location of in situ data from the CORA v5.0 for year 2012 as received by the Coriolis data Centre and illustrates the paucity of data in the Arctic region. Blue data points represent Argo data while the red points are from other sources (e.g., XBT, CTD, ship etc.). Also indicated are various seas in the region as well as the mouth of key rivers. Panels b-c illustrate dependence of T_B in the V and H polarizations to SST at different SSS ranging from 25-29 psu at 1.43 GHz frequency and 35° incidence angle.

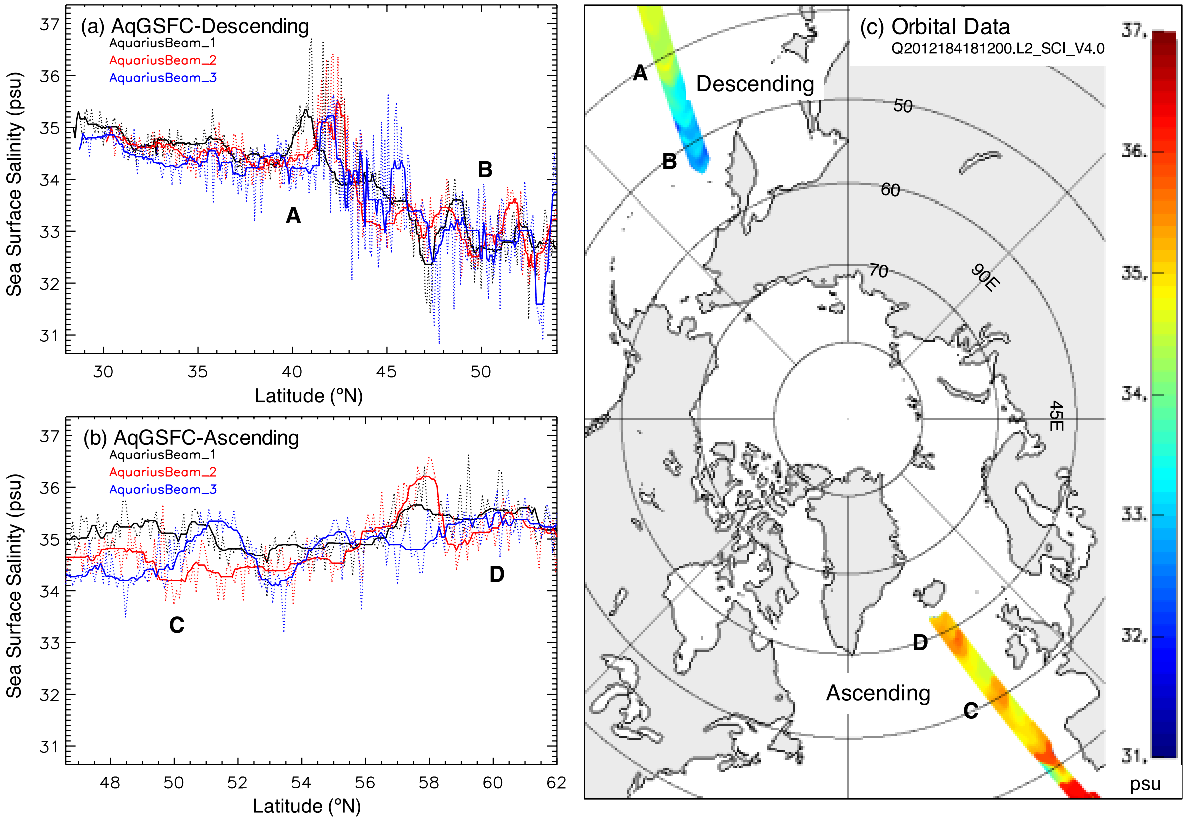

Figure 2. Aquarius Level-2 SSS three beams (dotted line: Beam1-black; Beam2-red; Beam3-blue) passing through North Atlantic (Ascending) and North Pacific (Descending) starting at 6:12PM UTC on July 2, 2012. Solid line show result after applying median filter along track with window of 9 observations.

Figure 3. Polarstern track from (a) 15 June – 06 October 2012 and (b) 08 June – 04 October 2014, covering Norwegian Sea, Greenland Sea, Fram Strait, Arctic Ocean, Barents Sea and Laptev Sea. Letters A-D in 2012 and E-G in 2014 are portions of the ship's tracks used for the validation of the satellite derived salinity measurements. Tick marks of varied shapes indicate extent of each segment used.

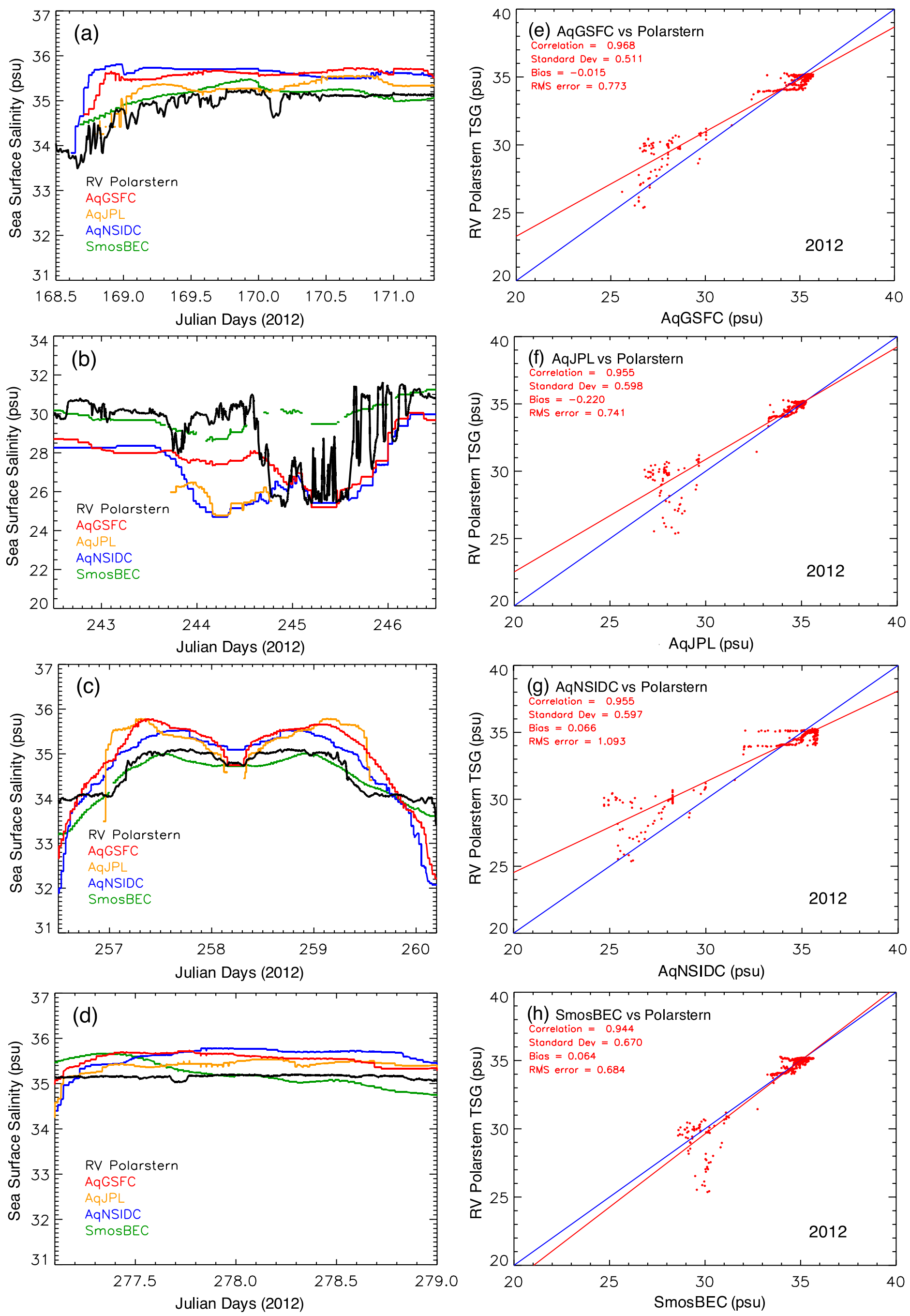

Figure 4. Comparison of Polarstern TSG measurements (black) versus collocated satellite-derived SSS products namely: AqGSFC (red), AqJPL (orange), AqNSIDC (blue), and SmosBEC (green) from 15 June – 06 October 2012. Areas (a-d) are segments of the ship tracks that are not

contaminated by sea ice or land as illustrated in Figure 3. Scatter plots of co-located (a) AqGSFC; (b) AqJPL; (c) AqNSIDC; and (d) SmosBEC versus Polarstern TSG measurements for the same period.

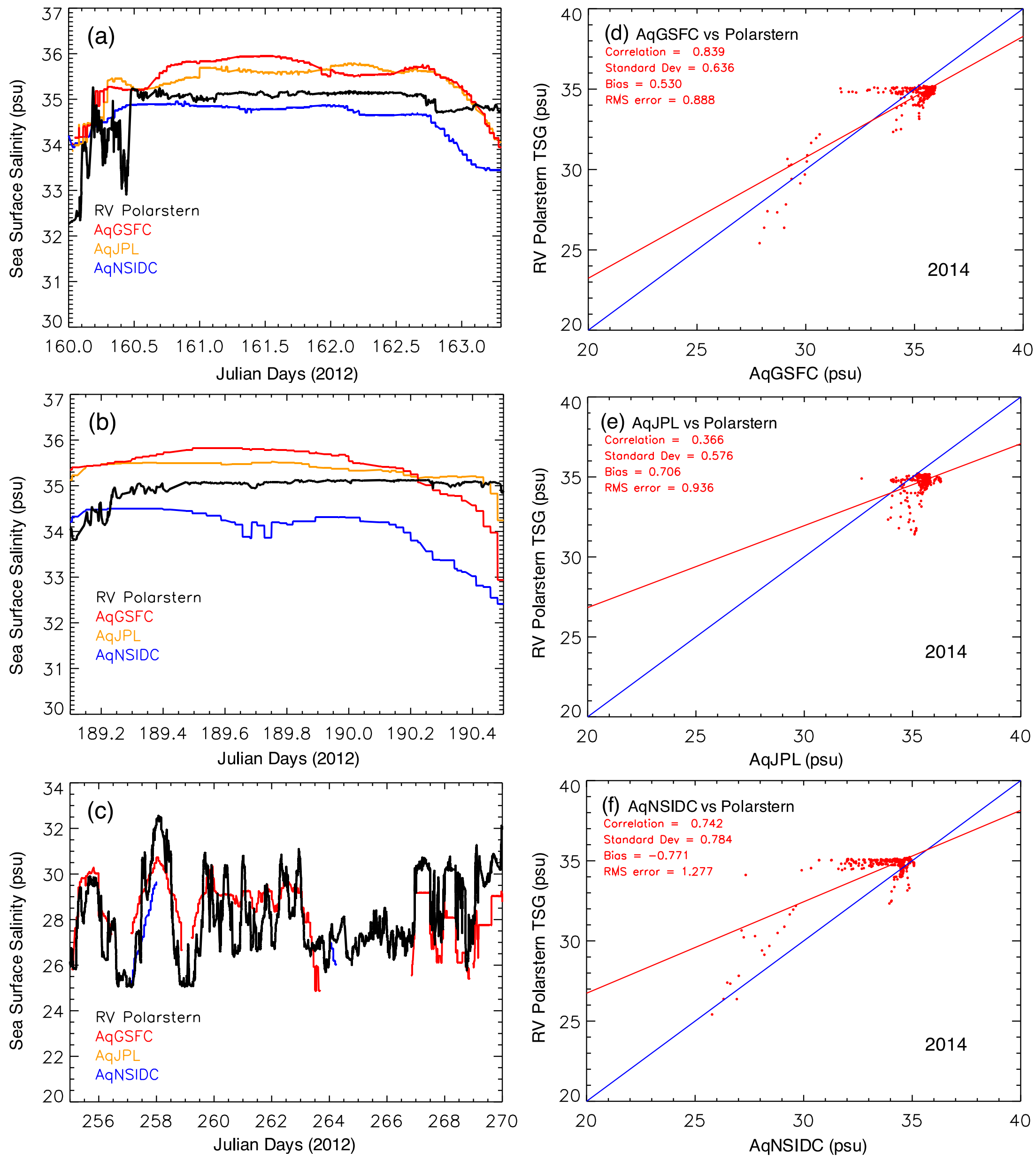

Figure 5. Comparison of Polarstern TSG measurements (black) versus collocated satellite-derived SSS measurements from AqGSFC (red), AqJPL (orange), AqNSIDC (blue), and SmosBEC (green) from 08 June – 04 October 2014**.** Areas (a-d) were highlighted due to the absence of possible contamination from sea ice and land. Scatter plots of co-located (a) AqGSFC; (b) AqJPL; and (c) AqNSIDC versus Polarstern TSG measurements for the same period.

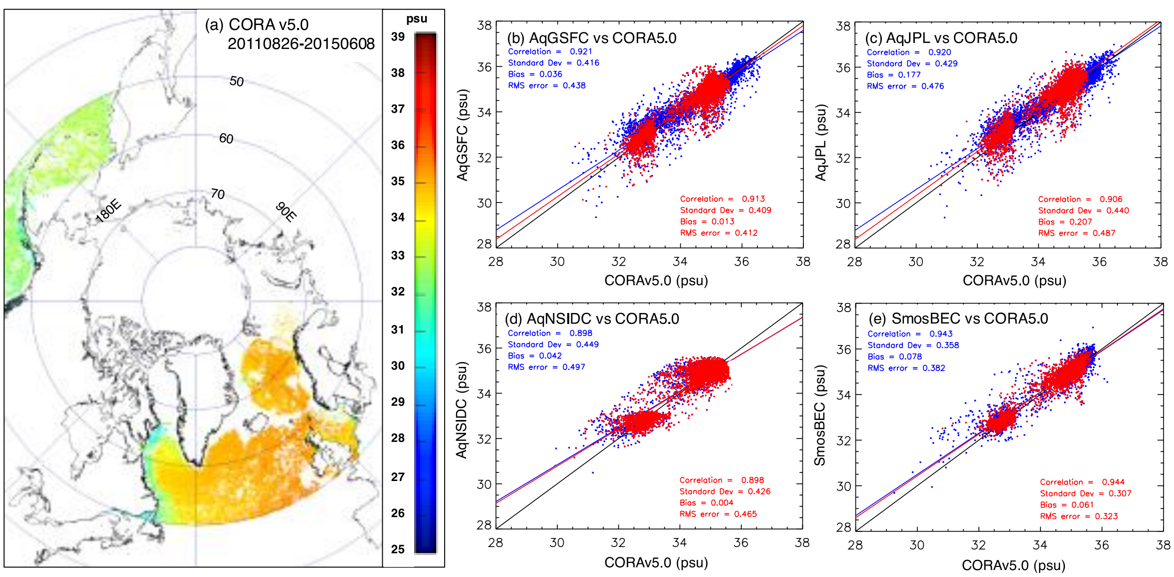

Figure 6. In situ SSS map from 26 August 2011 to 06 June 2015 using (a) CORA5.0 and scatter plots of collocated satellite-derived SSS data from (b) AqGSFC, (c) AqJPL, (d) AqNSIDC, and (e) SmosBEC versus CORA5.0. Scatterplots of each of the products with CORA5.0 are shown in blue while data points common among all the products with CORA5.0 are shown in red.

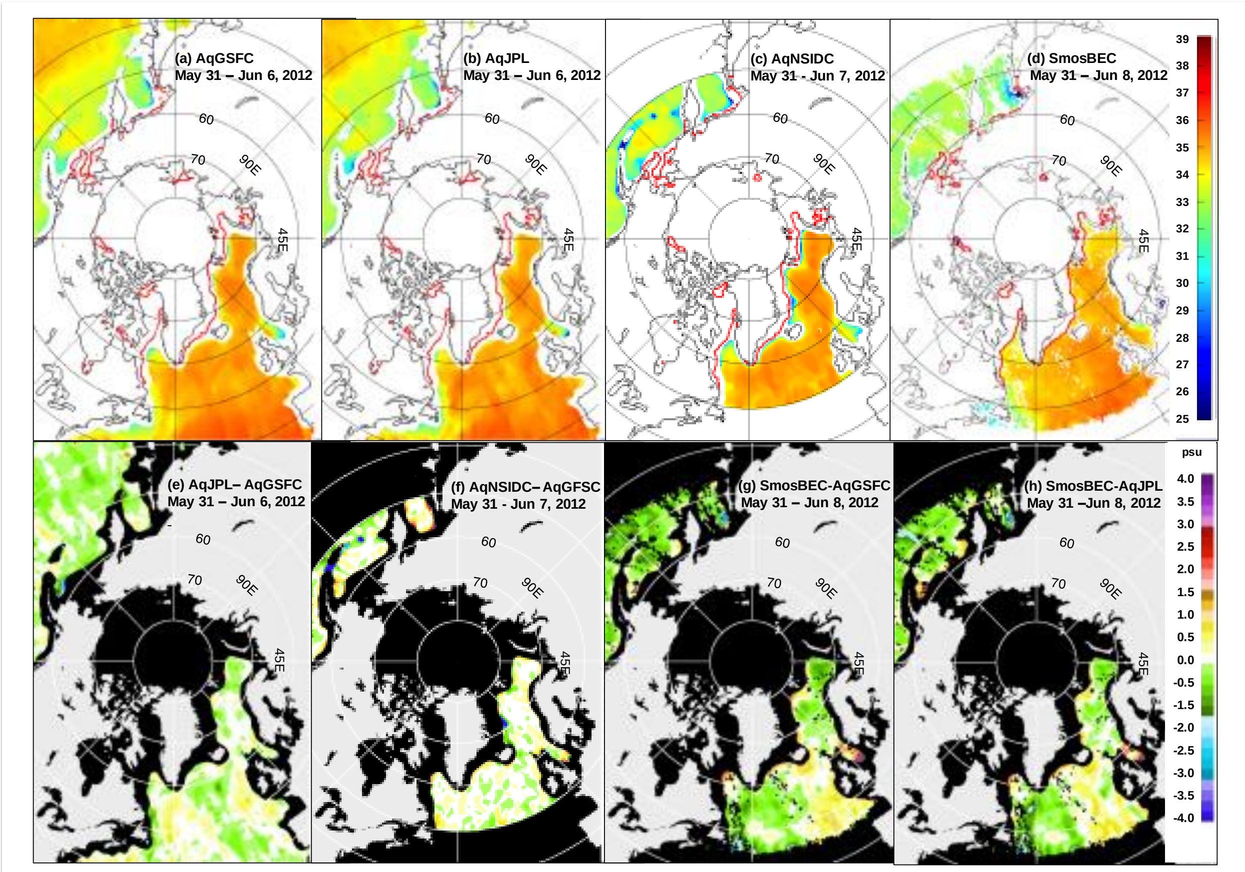

Figure 7. Difference map (e) shows the difference between processed (a) AqGSFC from (b) AqJPL; difference map (f) is the difference between (a) AqGSFC and (c) AqNSIDC; difference map (g) between (a) AqGSFC and (d) SmosBEC; and difference map (h) is the between (b) AqJPL and (d) SmosBEC all in the middle of spring of 2012.

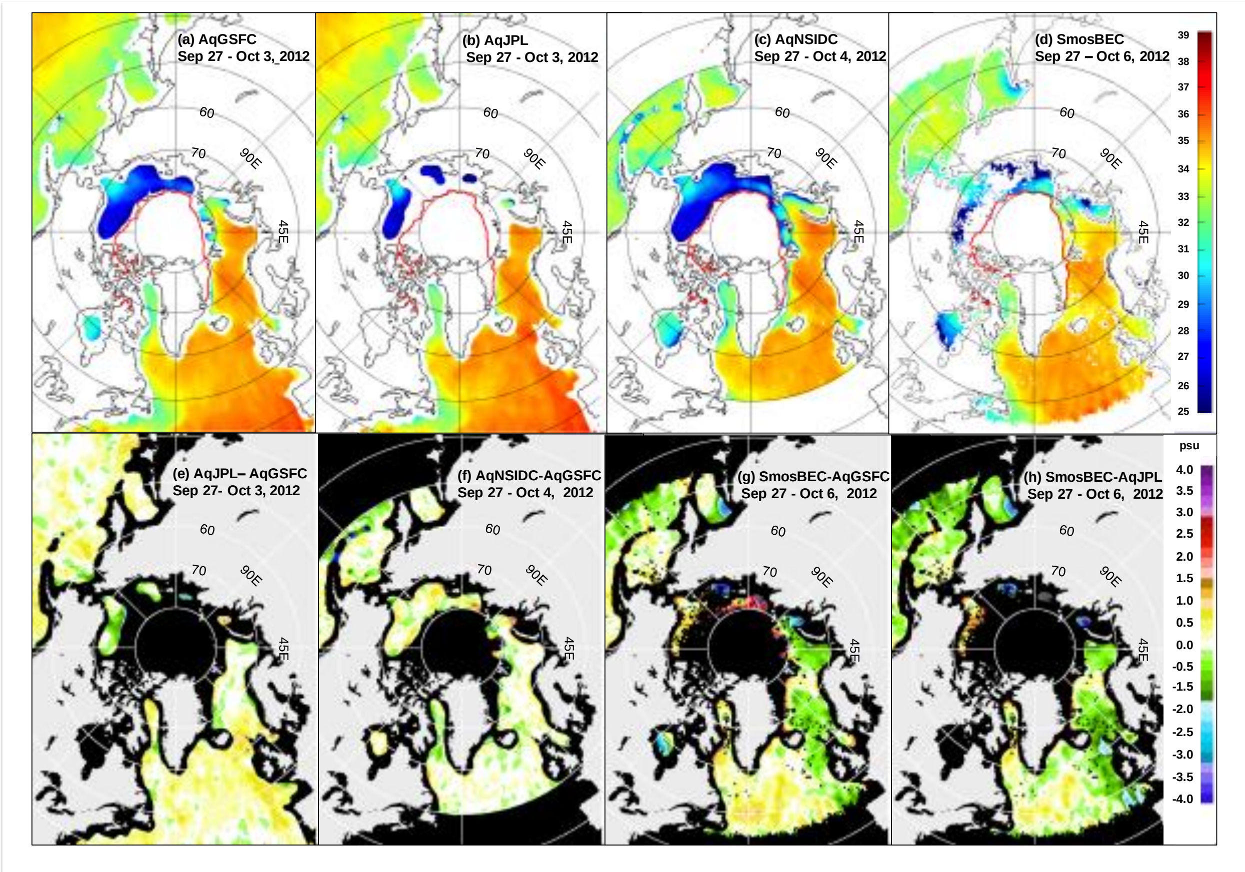

Figure 8. Difference map (e) shows the difference between processed (a) AqGSFC from (b) AqJPL (b); difference map (f) is the difference between (a) AqGSFC and (c) AqNSIDC ; difference map (g) between (a) AqGSFC and (d) SmosBEC; and difference map (h) is the between (b) AqJPL and (d) SmosBEC all in the end of early autumn of 2012.

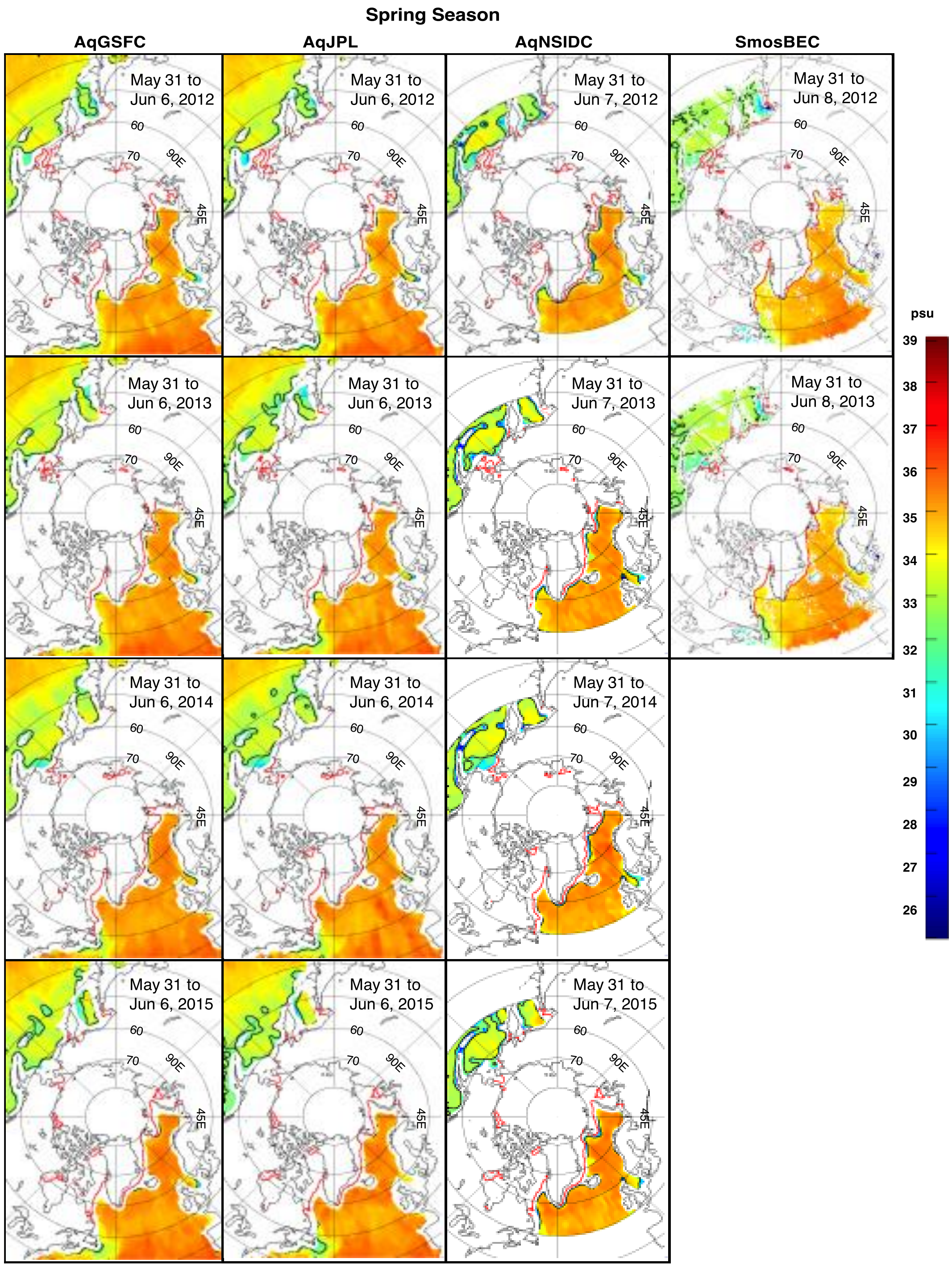

Figure 9. Inter-annual SSS distribution in spring of 2011-2015 from (a) AqGSFC, (b) AqJPL, (c) AqNSIDC and (d) SmosBEC product from 2012-2013. Also shown are 33 psu contours in black.

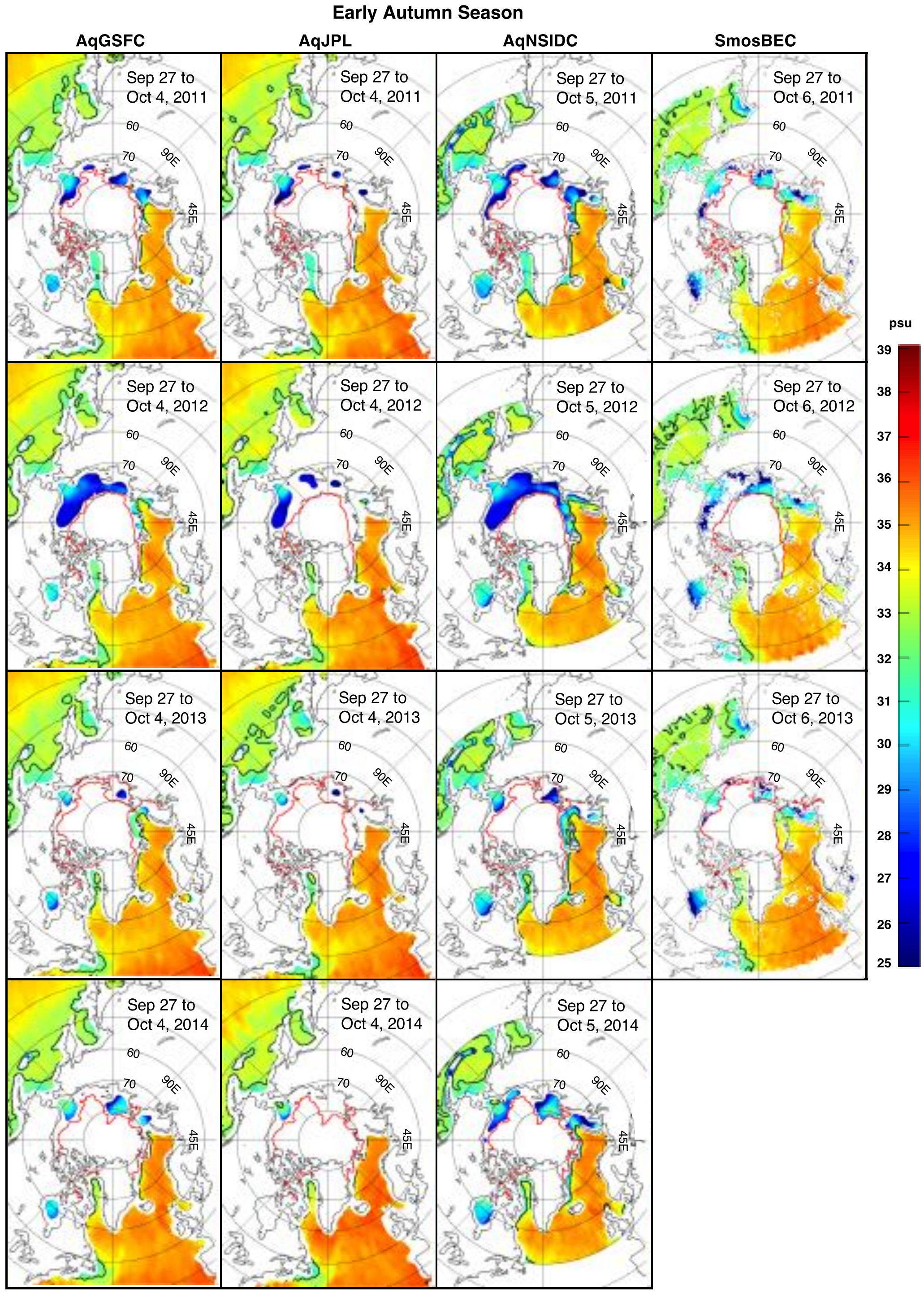

Figure 10. Inter-annual SSS distribution in early autumn 2011-2014 from (a) AqGSFC, (b) AqJPL, (c) AqNSIDC and (d) SmosBEC product from 2011-2013. Also shown are 33 psu contours in black.

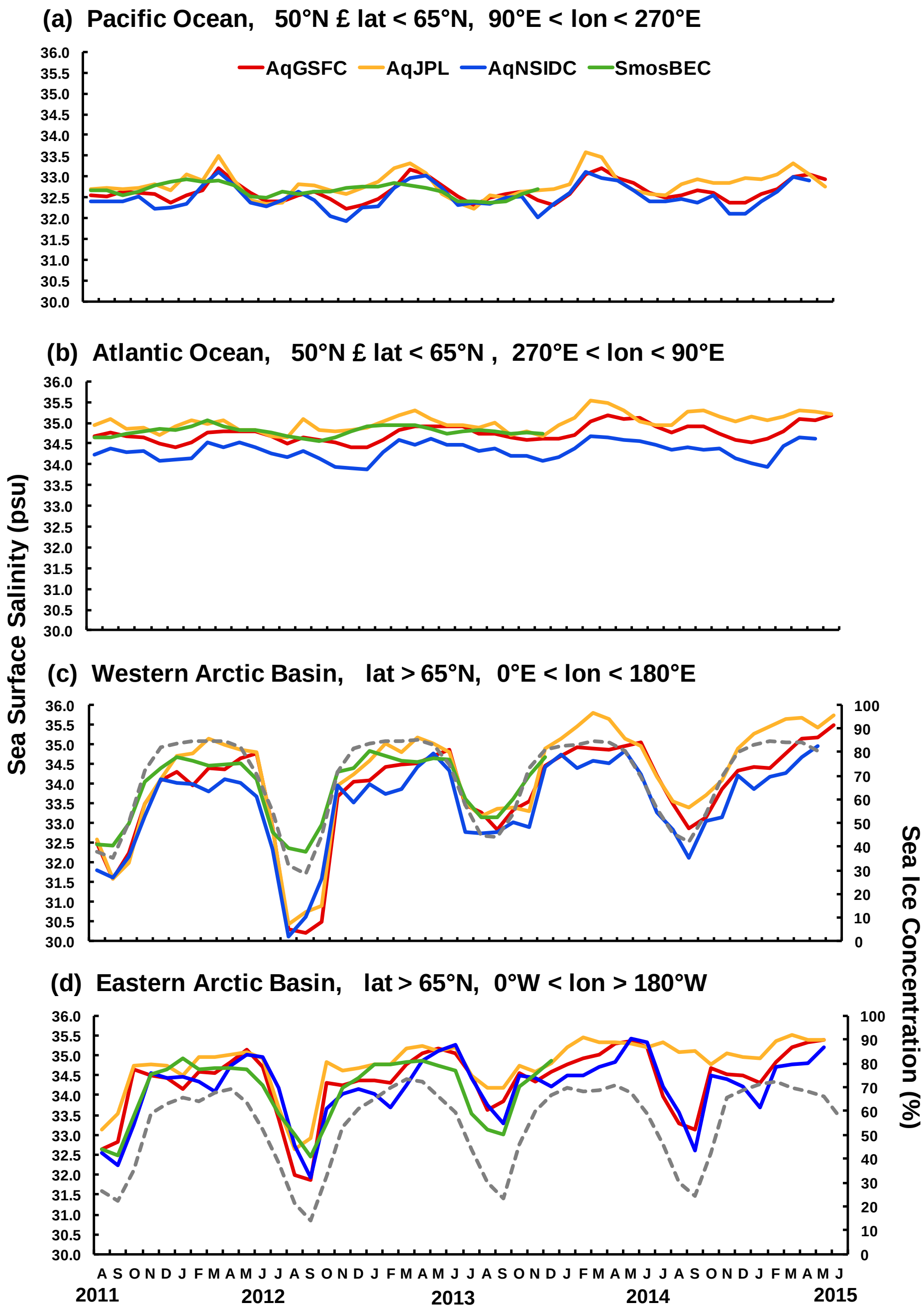

Figure 11. Monthly SSS averages of AqGSFC (red), AqJPL (yellow), AqNSIDC (blue) from August 2011 to June 2015 and SmosBEC from August 2011 to December 2013 in the (a) Pacific Ocean (> 50°N, < 65°N, < 270°E, > 90°E), Atlantic Ocean (> 50°N, < 65°N, < 90°E, > 270°E),

Western Arctic Basin (> 65°N, < 180°E, > 0°E), and Eastern Arctic Basin (> 65°N, > 180°W, > 0°W). SB2 sea ice concentration monthly averages plotted on c-d are shown as the gray dashed line.